DØ Note 5916-CONF

Limits on Anomalous Trilinear Gauge Boson Couplings from $WW + WZ \to l\nu jj$ events from $p\bar{p}$ collisions at $\sqrt{s} = 1.96$ TeV

The DØ Collaboration
URL http://www-d0.fnal.gov
(Dated: April 24, 2009)

This paper describes a measurement of the anomalous trilinear gauge boson couplings at the γWW and ZWW vertices. We study WW and WZ events produced in $p\bar{p}$ collisions at $\sqrt{s} = 1.96$ TeV, considering events with one electron or one muon, missing transverse energy, and at least two jets. The data samples were collected in RunIIa by the DØ detector and correspond to 1.07 fb^{-1} of integrated luminosity each for the electron+jets and muon+jets channels. Assuming two different relations between the anomalous coupling parameters $\Delta\kappa_\gamma$, $\Delta\lambda$ and Δg_1^Z, we set the 95% C.L. limits to be $-0.44 < \Delta\kappa_\gamma < 0.55$, $-0.10 < \Delta\lambda < 0.11$ and $-0.12 < \Delta g_1^Z < 0.20$ in the "LEP parametrization" scenario and $-0.16 < \Delta\kappa < 0.23$ and $-0.11 < \Delta\lambda < 0.11$ in the "Equal couplings" scenario.

Preliminary Results for Spring 2009 Conferences

I. INTRODUCTION

The simultaneous production of two weak vector bosons is a process involved in a large number of measurements at the Tevatron collider. A primary motivation for studying diboson physics is that their production and interactions provide a test of the electroweak sector of the Standard Model (SM). In $p\bar{p}$ collisions the diboson production process provides the handle to study the interactions between vector bosons since it receives contributions from the vertex involving the trilinear gauge boson couplings (TGCs) [1]. Any deviation of TGCs from their predicted SM values could be an indication for new physics (NP) beyond the SM and could give us some clues about the electroweak symmetry breaking mechanism (EWSB). The study of the production of WW, and WZ states has focussed dominantly on the purely leptonic final states [2, 3]. For the $WW + WZ$ cross section measurement in the $l\nu jj$ final state we refer to the accepted publication [4] and we describe the TGCs measurements in the same final state studied in this note. The latest combined results from the LEP experiments [5] report higher precision of measured couplings than those measured at the Tevatron. Due to the full reconstruction of the event kinematics in the e^+e^- collisions, higher signal selection efficiencies and smaller background contamination, the increased statistics results in higher sensitivities to anomalous couplings.

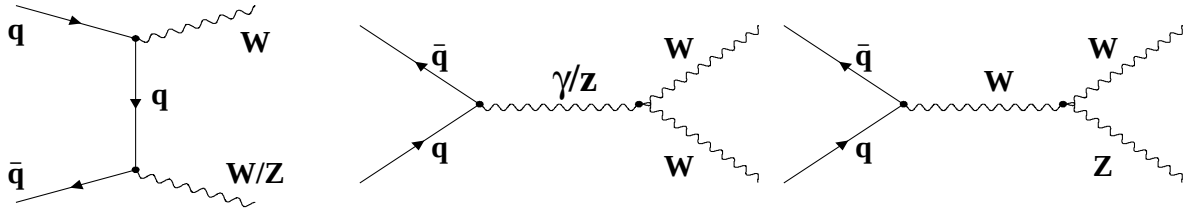

FIG. 1: Tree level Feynman diagrams for the processes of the WW/WZ production at the Tevatron collider via t-channel exchange (left) and s-channel exchange (middle and right).

As shown in the tree-level Feynman diagrams of Fig. 1, the TGCs contribute to $W^+W^-/W^\pm Z^0$ production via s-channel exchange diagrams while the t-channel diagram dominates the total cross section. The s-channel contains a trilinear gauge boson vertex γWW and/or ZWW depending on whether WW or WZ pairs are produced. Because the Z boson does not couple to neutral gauge bosons, WZ production can only probe the ZWW vertex, while WW production receives contributions from both the γWW and ZWW vertices.

II. PHENOMENOLOGY

The origin of EWSB and the mass generation mechanism are some of the biggest challenges of the SM today. The SM introduces an effective Higgs potential with an upper limit on the Higgs boson mass of ≈ 800 GeV to prevent tree-level unitarity violation. The unitarity bound indicates the mass scale at which the SM must be superseded by some kind of new physics. For heavier Higgs boson masses (or in the Higgsless scenario) the NP (e.g. the new strong dynamics [6]) must take its place in order to restore the unitarity at TeV energies and the SM is considered as a low-energy approximation of another theory. Conversely, if a light Higgs boson exists, the SM may nevertheless be incomplete, and NP could appear at higher energies. The effects of this larger theory are contained in the effective low energy Lagrangian expanded in powers of $(1/\Lambda_{NP})$ as:

$$\mathcal{L}_{eff} = \sum_{n\geq 0}\sum_{i}\frac{\alpha_i^n}{{\Lambda_{NP}}^n}O_i^{(n+4)} = \mathcal{L}_{eff}^{SM} + \sum_{n\geq 1}\sum_{i}\frac{\alpha_i^n}{{\Lambda_{NP}}^n}O_i^{(n+4)}, \quad (1)$$

where Λ_{NP} is the energy scale of the NP. The coefficients α_i parameterize all possible effects at low energies and the effective Lagrangian (Eq. 1) parameterizes the low energy effects of the NP at higher energies in a model-independent way. Since the NP scale is above the energies available in the experiments, the NP effects might not be observed directly, but they can affect measured observables like the gauge boson self-interactions. For the study of the gauge boson self-interactions, the relevant terms in the Lagrangian (Eq. 1) are those that produce vertices with three or four gauge bosons. The effective Lagrangian that parameterizes the most general Lorentz invariant WWV vertex

$(V = Z, \gamma)$, involving two W bosons is defined as [7]:

$$\begin{aligned}\frac{\mathcal{L}_{eff}^{WWV}}{g_{WWV}} &= ig_1^V(W_{\mu\nu}^* W^\mu V^\nu - W_\mu^* V_\nu W^{\mu\nu}) + i\kappa_V W_\mu^* W_\nu V^{\mu\nu} + i\frac{\lambda_V}{M_W^2} W_{\lambda,\mu}^* W_\nu^\mu V^{\nu\lambda} - g_4^V W_\mu^* W_\nu(\partial^\mu V^\nu + \partial^\nu V^\mu) \\ &+ g_5^V \epsilon^{\mu\nu\lambda\rho}(W_\mu^* \partial_\lambda W_\nu - \partial_\lambda W_\mu^* W_\nu)V_\rho + i\tilde{\kappa}_V W_\mu^* W_\nu \tilde{V}^{\mu\nu} + i\frac{\tilde{\lambda}_V}{M_W^2} W_{\lambda\mu}^* W_\nu^\mu \tilde{V}^{\nu\lambda},\end{aligned} \tag{2}$$

where $\epsilon_{\mu\nu\lambda\rho}$ is the fully antisymmetric ϵ - tensor, W denotes the W boson field, V denotes the photon or Z boson field, $V_{\mu\nu} = \partial_\mu V_\nu - \partial_\nu V_\mu$, $W_{\mu\nu} = \partial_\mu W_\nu - \partial_\nu W_\mu$, $\tilde{V}_{\mu\nu} = 1/2(\epsilon_{\mu\nu\lambda\rho} V^{\lambda\rho})$, $g_{WW\gamma} = -e$ and $g_{WWZ} = -e\cot\theta_W$, where $\sin^2\theta_W$ is the weak mixing angle. The fourteen coupling parameters of WWV vertices are grouped according to their symmetries as C (charge conjugation) and P (parity) conserving couplings (g_1^V, κ_V and λ_V), C and P violating but CP conserving couplings (g_5^V) and CP violating couplings ($g_4^V, \tilde{\kappa}_V$ and $\tilde{\lambda}_V$). In the SM all couplings vanish ($g_5^V = g_4^V = \tilde{\kappa}_V = \tilde{\lambda}_V = 0$) except $g_1^V = \kappa_V = 1$. The value of g_1^γ is fixed by the electro-magnetic gauge invariance ($g_1^\gamma = 1$ for on-shell photons) while the value of g_1^Z may differ from its SM value. Considering the C and P conserving couplings only, the deviations from the SM values are denoted as the *anomalous* TGCs (ATGCs) Δg_1^Z $(= g_1^Z - 1)$, $\Delta\kappa_\gamma = (\kappa_\gamma - 1)$, $\Delta\kappa_Z = (\kappa_Z - 1)$, $\Delta\lambda_\gamma$ $(= \lambda_\gamma - 0)$ and $\Delta\lambda_Z$ $(= \lambda_Z - 0)$. If the ATGCs are introduced in the effective Lagrangian (Eq. 1), their increase will unphysically increase the WW and WZ production cross sections as the partonic constituents center-of-mass energy $\sqrt{\hat{s}}$ approaches to Λ_{NP} and divergences would violate unitarity. Divergences in the cross section are canceled out by introducing a form factor:

$$\alpha(\hat{s}) \rightarrow \frac{\alpha_0}{(1 + \hat{s}/\Lambda_{NP}^2)^2}, \tag{3}$$

for which the anomalous coupling vanishes as $\hat{s} \rightarrow \infty$. The value of Λ_{NP} used to set anomalous coupling limits for a given coupling parameter α is the highest value possible before the unitarity limit is tighter than the coupling limits set by data. Theoretical arguments suggest that the ATGCs are at most of $\mathcal{O}(M_W^2/\Lambda_{NP}^2)$ which implies that for $\Lambda_{NP} \sim 1$ TeV the ATGCs are expected to be of $\mathcal{O}(10^{-2})$. As the NP scale increases, the effects on ATGCs are less than $\mathcal{O}(10^{-2})$ and their observation needs either more precise measurements or higher center-of-mass energies.

Interpretation of the effective Lagrangian (Eq. 1), depends on the specified symmetry and the particle content of the low energy theory. In the light Higgs boson scenario, the low-energy spectrum is augmented by the Higgs boson and the NP is described using a linear realization of the symmetry. Including the scalar Higgs doublet field, considering operators up to dimension-6 only and retaining $SU(2) \times U(1)$ gauge invariance, the effective Lagrangian can be written in terms of the operator coefficients α_i [8] where the NP scale Λ_{NP} is replaced by the W boson mass. In this so-called "LEP parameterization", the relations between the C and P conserving TGCs then become:

$$\Delta\kappa_Z = \Delta g_1^Z - \Delta\kappa_\gamma \cdot \tan^2\theta_W \;\text{ and }\; \lambda_Z = \lambda_\gamma = \lambda, \tag{4}$$

Hereafter in the text we will refer to this parametrization as the "LEP parametrization" with 3 different parameters, κ_γ, λ and g_1^Z. The coupling κ_Z can be expressed via the relation given by Eq. 4. If the light Higgs boson is absent or sufficiently heavy the effective Lagrangian should be expressed using a nonlinear realization of the symmetry [9] to prevent unitarity violation. The description of self-couplings relies on the chiral Lagrangian [10] where the Higgs doublet field is replaced by the Goldstone bosons and the scale $\Lambda_{NP} = 4\pi v$. The assumption is that only $SU(2)_L \times U(1)_Y$ gauge fields, fermions and would-be Goldstone bosons are present and unitarity is restored by the strong EWSB mechanism while the NP effects should appear at a scale below 3 TeV.

The second scenario is called the "Equal couplings" scenario [1], where the γWW and ZWW couplings are set equal to each other. This is also relevant for studying interference effects between the photon and Z-exchange Feynman diagrams in WW production (Fig.1). In this case, electromagnetic invariance sets $\Delta g_1^Z = \Delta g_1^\gamma = 0$, since it forbids any deviation of g_1^γ from its SM value and the relations between the couplings become:

$$\Delta\kappa_Z = \Delta\kappa_\gamma \;\text{ and }\; \lambda_Z = \lambda_\gamma = \lambda, \tag{5}$$

Besides the different scenarios previously mentioned, one can always probe the couplings assuming that there is no constraint between κ, λ and g_1. In the following analysis we assume "LEP parametrization" and "Equal couplings" scenarios and set the limits on $\Delta\kappa, \Delta\lambda$ and Δg_1 as if there are existing relations given by Eq. 4 or Eq. 5, respectively. As already stated, in WW and WZ production the anomalous couplings contribute to the total cross section via the s-channel exchange diagram. Anomalous couplings enter the differential production cross sections and give a contribution to different helicity amplitudes which are proportional to the center-of-mass energy squared $\hat{s}$. Thus, at a given $\hat{s}$ the sensitivity to the coupling λ is higher because it is multiplied by $\hat{s}$ in amplitudes for WW and WZ production. The coupling κ is not directly related to $\hat{s}$ or it is multiplied by $\sqrt{\hat{s}}$ depending on the process. Besides,

λ mostly affects transversely polarized gauge bosons which mainly contribute to the total cross section. Thus, we expect higher sensitivity to λ than to κ couplings. A different sensitivity to the κ couplings depends on the choice of the scenario as well. The sensitivity to the κ coupling in the "Equal couplings" scenario is higher than in the "LEP parametrization" scenario, simply because of the different relations in Eq. 4 and Eq. 5.

We simulate the effects of anomalous trilinear gauge couplings by reweighting the predictions for WW and WZ production from the PYTHIA [11] MC generator to match those made by Hagiwara, Zeppenfeld and Woodside (LO) Monte Carlo (MC) generator (HZW) [12] which takes the effects of anomalous couplings into account. The reweighting method uses the calculated matrix element values to predict the rate at which a given event would be generated in the presence of anomalous couplings. The rate represents an event weight R. Since the HZW generator does not recalculate matrix elements, we use high statistics samples to calculate the weight as a function of anomalous coupling. Thus, we consider our approach as a very close approximation of the exact reweighting method. The basis of this method is that the equation of the differential cross section, which has a quadratic dependence on the anomalous couplings can be written as:

$$\begin{aligned} d\sigma &= const \cdot |\mathcal{M}|^2 dX \\ &= const \cdot |\mathcal{M}|^2_{SM} \tfrac{|\mathcal{M}|^2}{|\mathcal{M}|^2_{SM}} dX \\ &= const \cdot |\mathcal{M}|^2_{SM} [1 + A(X)\Delta\kappa + B(X)\Delta\kappa^2 + C(X)\Delta\lambda + D(X)\Delta\lambda^2 + E(X)\Delta\kappa\Delta\lambda + ...] dX \\ &= d\sigma_{SM} \cdot R(X; \Delta\kappa, \Delta\lambda, ...) \end{aligned} \tag{6}$$

where $d\sigma$ is the differential cross section which includes the contribution from the anomalous couplings, $d\sigma_{SM}$ is the SM differential cross section, X is a kinematic distribution sensitive to the anomalous couplings and A, B, C, D and E are reweighting coefficients dependent on X. Consequently, Eq. 6 in the "Equal couplings" scenario is parameterized with 2 couplings, $\Delta\kappa$ and $\Delta\lambda$, and 5 reweighting coefficients, $A(X), B(X), C(X), D(X)$ and $E(X)$. In the "LEP parametrization", scenario, Eq. 6 is parameterized with 3 couplings $\Delta\kappa_\gamma, \Delta\lambda$ and Δg_1^Z and 9 reweighting coefficients $A(X), B(X), C(X), D(X), E(X), F(X), G(X), H(X)$ and $I(X)$. The kinematic distribution X is chosen to be the p_T of the $q\bar{q}$ system, which has the highest sensitivity to anomalous couplings, as shown in Fig. 2. Depending on the number of reweighting coefficients, a system of the same number of equations allows us to calculate their values for each event. Applied on the SM distribution X with any combination of anomalous couplings, the distribution X weighted by R corresponds to the kinematic distribution X in the presence of a non-SM coupling according to Eq. 6.

To calculate reweighting coefficients, we generate 9 ("LEP parameterization") and 5 ("Equal couplings") different R functions combining the shape information from the $p_T^{q\bar{q}}$ distributions in the presence of anomalous couplings with $\Delta = \pm\ 0.5$ relative to the SM. Once the weights R are properly normalized using the the cross sections given by the generator, we derive the reweighting coefficients in the "LEP parameterization" as a function of $p_T^{q\bar{q}}$ as:

$$\begin{aligned} C(X) &= (R_1 - R_2)/2\Delta\lambda \\ D(X) &= (R_1 + R_2 - 2)/2\Delta\lambda^2 \\ A(X) &= (R_3 - R_4)/2\Delta\kappa \\ B(X) &= (R_3 + R_4 - 2)/2\Delta\kappa^2 \\ E(X) &= (R_5 - R_6)/2\Delta g_1 \\ F(X) &= (R_5 + R_6 - 2)/2\Delta {g_1}^2 \\ G(X) &= (R_7 - 1 - A(X)\Delta\kappa - B(X)\Delta\kappa^2 - C(X)\Delta\lambda - D(X)\Delta\lambda^2)/\Delta\kappa\Delta\lambda \\ H(X) &= (R_8 - 1 - A(X)\Delta\kappa - B(X)\Delta\kappa^2 - E(X)\Delta g_1 - F(X)\Delta {g_1}^2)/\Delta\kappa\Delta g_1 \\ I(X) &= (R_9 - 1 - C(X)\Delta\lambda - D(X)\Delta\lambda^2 - E(X)\Delta g_1 - F(X)\Delta {g_1}^2)/\Delta\lambda\Delta g_1, \end{aligned} \tag{7}$$

where R_{1-9} are properly normalized event weights calculated with different sets of anomalous couplings $\Delta\kappa,\ \Delta\lambda$ and Δg_1, and all deviation are $\Delta = \pm\ 0.5$. In the "Equal couplings" scenario Eq. 7 consists of $A(X), B(X), C(X), D(X)$ and $E(X)$ with $E(X)$ taking a form of $G(X)$. As a cross check, we recalculate the weight R for different $\Delta\kappa, \Delta\lambda$ and/or Δg_1 with reweighting coefficients obtained from Eq. 7 and compare reweighted $p_T^{q\bar{q}}$ shapes to those predicted by the generator as shown in Fig. 4. Discrepancies in shape (for $p_T^{q\bar{q}} > 100$ GeV) within $\leq \pm 5\%$ and normalization $\leq 0.1\%$ from those predicted by the generator, represent good agreement and allow us to describe the effects of anomalous couplings using the approximated reweighting technique.

Thus, we generate three two-parameter grids by varying only two parameters in steps of 0.01 while the third one is fixed to its SM value. Events from both the electron and the muon channel are summed. For a given $(\Delta\kappa,\ \Delta\lambda)$, $(\Delta\kappa,\ \Delta g_1)$ and $(\Delta\lambda,\ \Delta g_1)$ combination each event in the reconstructed dijet p_T bin is weighted by its weight R and all the weighted events are summed in that bin.

III. SELECTION OF $WW/WZ \to l\nu jj$ CANDIDATE EVENTS

This analysis builds upon a previous analysis in which we reported the first evidence of WW/WZ production with lepton+jets final states at a hadron collider [13]. We will briefly summarize the previous analysis in this paragraph. We used 1.07 fb^{-1} of RunIIa DØ data to select events with two jets, an electron or muon, and significant missing transverse energy. The $e\nu q\bar{q}$ candidate events are required to pass a trigger based on a single electron or electron+jet(s). In the muon channel, we select all events in the available data sample which satisfy our kinematic selection requirements, with no specific trigger requirement. To select $WW/WZ \to \ell\nu q\bar{q}$ candidates, we require a reconstructed electron or muon with transverse momentum $p_T > 20$ GeV and pseudorapidity $|\eta| < 1.1$ (2.0) for electrons (muons), the imbalance in transverse energy to be $\not\!\!E_T > 20$ GeV and at least two jets with $p_T > 20$ GeV and $|\eta| < 2.5$. The jet of highest p_T must have $p_T > 30$ GeV. To reduce background from processes that do not contain $W \to \ell\nu$, we require a "transverse" mass of $M_T^{\ell\nu} > 35$ GeV. Signal (WW and WZ) and background (W+jets, Z+jets, $t\bar{t}$, single top and ZZ) processes are modeled using the MC simulation. All MC samples are normalized using next-to-leading-order (NLO) or next-to-next-to-leading-order predictions for SM cross sections, except the most dominant background W+jets which is scaled to the data. The multijet background events, in which the jet is misidentified as a lepton, is estimated from data. The signal and the backgrounds are further separated using a multivariate classifier Random Forest (RF) classifier [14, 15] to combine information from thirteen well-modeled kinematic variables. The signal cross section is determined from a fit of signal and background RF templates to the data by minimizing a Poisson χ^2 function with respect to variations in the systematic uncertainties, and it is measured to be 20.2 ± 2.5(stat) ± 3.6(syst) ± 1.2(lumi) pb. The measured yields for signal and each background are given in Table I.

TABLE I: Measured number of events for signal and each background after the combined fit (with total uncertainties determined from the fit) and the number observed in data.

	$e\nu q\bar{q}$ channel	$\mu\nu q\bar{q}$ channel
Diboson signal	436 ± 36	527 ± 43
W+jets	10100 ± 500	11910 ± 590
Z+jets	387 ± 61	1180 ± 180
$t\bar{t}$ + single top	436 ± 57	426 ± 54
Multijet	1100 ± 200	328 ± 83
Total predicted	12460 ± 550	14370 ± 620
Data	12473	14392

The WW and WZ events are generated with PYTHIA using the parton distribution functions (PDFs) CTEQ6L1 [16]. These events are corrected by a kinematically-dependent next-to-leading-order k-Factor, as described in Section VII of [4]. The WW and WZ production cross sections for the semileptonic final state generated with the HZW and normalized to the SM value, as a function of anomalous couplings are shown in Fig. 3. We vary only one coupling at a time leaving the others fixed at their SM values. The effects of ATGCs on different kinematic distributions (p_T of the $q\bar{q}$ system and angular distribution of the $q\bar{q}$ system) assuming the "LEP parametrization" are shown in Fig. 2 for WW and WZ events. Since the TGCs introduce terms in the Lagrangian which are proportional to the momentum of the boson $p^{W/Z}$, it is expected that in the presence of ATGCs the differential cross section $d\sigma/dp^{W/Z}$ deviates from the SM prediction. The same behavior is expected at large production angles of a boson. Thus, the W/Z boson transverse momentum $p_T^{W/Z} = p^{W/Z} sin\theta_{CM}^{W/Z}$ is sensitive to ATGCs and shows an enhancement of a number of events at high $p_T^{W/Z}$ values. Consequently, the differential cross section $d\sigma/dp_T^{W/Z}$ is sensitive to these changes too.

In the TGC analysis we use the reconstructed dijet p_T spectrum of selected $WW/WZ \to \ell\nu q\bar{q}$ candidates (instead of the RF output used in the previous analysis for the cross section measurement) defined as $p_T^{jj} = \sqrt{p_{x,jj}^2 + p_{y,jj}^2}$ (where $p_{x/y,jj}$ is the sum of the 4-vector x/y-components of the two most energetic jets in the event) to probe the data for the presence of the anomalous couplings $\Delta\kappa$, $\Delta\lambda$ and Δg_1^Z assuming the two different scenarios, "LEP parametrization" and "Equal couplings". All selection criteria and background estimates are the same as described in previous paragraph.

IV. SYSTEMATIC UNCERTAINTIES

The statistical analysis for this measurement considers two general types of systematic uncertainties. Uncertainties of the first class (TYPE I) are related to the overall normalization and efficiencies of the various contributing physical

processes. The second class (TYPE II) consists of uncertainties which impact the kinematic distributions, commonly referred to as shape uncertainties. Although TYPE II uncertainties may also impact efficiencies or normalization, any uncertainty shown to impact the shape of the dijet p_T distribution are treated as TYPE II.

All TYPE I uncertainties are determined via subsidiary data samples not included in this measurement. The largest contributing uncertainties are those related to the cross section factors used to normalize the background processes. These are related to the accuracy of the theoretical cross section calculation with the largest uncertainty being $20 \oplus 20 \approx 28\%$ for W/Z + heavy flavor jets cross sections. The remaining TYPE I uncertainties are associated with the luminosity measurement and the efficiencies for reconstructing and triggering on leptons. Unless otherwise specified, TYPE I uncertainties are considered to arise from Gaussian parent distributions.

The TYPE II uncertainties are those that, when propagated through the analysis selection, impact the shape of the dijet p_T distribution. Each TYPE II uncertainty is associated with a specific aspect of this analysis (e.g., the energy scale of jets) and its magnitude is determined outside this analysis unless otherwise specified. The dependence of the dijet p_T distribution on these uncertainties is determined by varying each parameter by its associated uncertainty ($\pm 1\sigma$) and re-evaluating the shape of the dijet p_T distribution. The resulting shape dependence is considered to arise from a Gaussian parent distribution. Both types of systematic uncertainty are assumed to be 100% correlated amongst backgrounds and signals. All sources of systematic uncertainty are assumed to be mutually independent, and no inter-correlation is propagated. A list of the systematic uncertainties used in this analysis can be found in Table II.

TABLE II: Systematic uncertainties in percent for Monte Carlo simulations and multijet estimates. Uncertainties are identical for both lepton channels except where otherwise indicated. The nature of the uncertainty, *i.e.*, whether it refers to a shape dependence (TYPE II) or just normalization (TYPE I), is also provided. [The values for uncertainties with a shape dependence correspond to the maximum amplitude of shape fluctuations in the dijet p_T distribution (0 GeV $< p_T <$ 300 GeV) after $\pm 1\sigma$ parameter changes.]

Source of systematic uncertainty	Diboson signal	W+jets	Z+jets	Top	Multijet	Nature
Trigger efficiency, electron channel	$+2/-3$	$+2/-3$	$+2/-3$	$+2/-3$		TYPE I
Trigger efficiency, muon channel	$+0/-5$	$+0/-5$	$+0/-5$	$+0/-5$		TYPE II
Lepton identification	± 4	± 4	± 4	± 4		TYPE I
Jet identification	± 1	± 1	± 1	$\pm <1$		TYPE II
Jet energy scale	± 4	± 7	± 5	± 5		TYPE II
Jet energy resolution	± 3	± 4	± 4	± 4		TYPE I
Luminosity	± 6.1	± 6.1	± 6.1	± 6.1		TYPE I
Cross section		± 20	± 6	± 10		TYPE I
Multijet normalization, electron channel					± 20	TYPE I
Multijet normalization, muon channel					± 30	TYPE I
Multijet shape, electron channel					± 7	TYPE II
Multijet shape, muon channel					± 10	TYPE II
Diboson signal NLO/LO shape	± 10					TYPE II
Diboson signal ATGC reweighting	± 5					TYPE II
Parton distribution function	± 1	± 3	± 2	± 2		TYPE II
ALPGEN η and ΔR corrections		± 1	± 1			TYPE II
Renormalization and factorization scale		± 1	± 1			TYPE II
ALPGEN parton-jet matching parameters		± 1	± 1			TYPE II

V. ANOMALOUS COUPLING LIMITS

The 68% C.L. and 95% C.L. contour plots (observed limits) in two-parameter space are shown in Fig. 5 and Fig. 6 as a function of anomalous couplings. The most probable values of the anomalous couplings $\Delta\kappa$, $\Delta\lambda$ and Δg_1^Z as measured in data are shown by the black dots. The limits are obtained from the fits of different MC predictions in the presence of anomalous couplings to data, using the dijet p_T distributions of candidate events. We assume two different relations between the anomalous couplings ("LEP Parametrization" and "Equal Couplings") and $\Lambda_{NP} =$ 2 TeV. The observed limits are determined by a "best fit" of the signal and background templates to the observed data. More specifically, the fit utilizes the MINUIT [17] software package to minimize a Poisson χ^2 with respect to variations to the systematic uncertainties as explained in DØ Note 5309 [18]. The used χ^2 function is:

$$\chi^2 = -2\ln\left(\prod_i^{Nbins}\frac{\mathcal{L}^P(\mathrm{d_i};\mathrm{m'_i})}{\mathcal{L}^P(\mathrm{d_i};\mathrm{d_i})}\prod_k^{Nsyst}\frac{\mathcal{L}^G(R_k\sigma_k;\sigma_k)}{\mathcal{L}^G(0;\sigma_k)}\right) = 2\sum_i^{\mathrm{Nbins}}\mathrm{m'_i} - \mathrm{d_i} - \mathrm{d_i}\ln\left(\frac{\mathrm{m'_i}}{\mathrm{d_i}}\right) + \sum_{\mathrm{k}}^{\mathrm{Nsyst}}\mathrm{R_k^2} \quad (8)$$

where $\mathcal{L}^P(k;\lambda)$ is the discrete Poisson likelihood for k events with a mean value of λ events; $\mathcal{L}^G(\alpha;\sigma)$ is the likelihood for a variation from the mean value of α in a unit Gaussian distribution with variance σ; $\mathrm{d_i}$ is the number of data events in bin i and $\mathrm{m'_i}$ is the systematically varied prediction for the number of MC events in bin i. The product and sum in k runs over the number of systematic uncertainties. Systematics are treated as Gaussian-distributed uncertainties on the expected numbers of signal and background events. The individual background contributions are fitted to the data by minimizing this χ^2 function over the individual systematic uncertainties [18]. The fit computes the optimal central values for the systematic uncertainties, while accounting for departures from the nominal predictions by including a term in the χ^2 function which sums the squared deviation of each systematics in units normalized by its $\pm1\sigma$ uncertainties.

Fig. 7 shows the dijet p_T distributions in the electron, muon and combined channels after the fit, along with the ±1 standard deviation systematic uncertainty on the background and the residual distance between the data points and the extracted signal, divided by the total uncertainty on the MC.

The observed 68% and 95% C.L. one-parameter limits, presented numerically in Table III are estimated from the single parameter fit with the second parameter fixed at its SM value. The $\Delta\chi^2$ values of 1 and 3.84 represent 68% C.L. and 95% C.L. single parameter limits respectively, where the $\Delta\chi^2$ is measured between data and MC distributions as the MC is varied in the presence of anomalous couplings. Assuming the "LEP parameterization" the most probable values as estimated from data are 1.07, 0.00 and 1.04 for κ_γ, λ and g_1^Z, respectively. For the "Equal couplings" scenario the most probable values as estimated from data are 1.04 and 0.00 for κ and λ, respectively.

As one can see from Table IV, the 95% C.L limits on anomalous couplings $\Delta\kappa_\gamma$, $\Delta\lambda$ and Δg_1^Z set using the dijet p_T distribution of $WW/WZ \to l\nu jj$ events are tighter than the 95% C.L limits set in the DØ WW [19] and WZ [20] analyses which use the fully leptonic channels. The 95% C.L. limits estimated in the DØ $W\gamma$ [21] analysis are comparable to our result. The combined LEP results still represent the world's tightest limits on charged anomalous couplings [22–25]. The combination of all four LEP experiments' results gives the most probable values of κ_γ, λ and g_1^Z as $\kappa_\gamma = 0.943^{+0.055}_{-0.055}$, $\lambda = -0.020^{+0.024}_{-0.024}$ and $g_1^Z = 0.998^{+0.023}_{-0.025}$ [5] at 68% C.L.

The presented measurement in $l\nu jj$ final states is limited by statistics. With additional data the sensitivity to anomalous couplings will approach the sensitivity of the individual LEP experiments [22–25] shown in Table V. With the luminosity of 4 fb^{-1} of data already recorded by DØ the sensitivity to the λ coupling is expected to be comparable to the sensitivity of a single LEP experiment. The limits on the κ_γ and g_1^Z couplings are expected to be less than two times those of the individual LEP experiments.

TABLE III: The observed 68% and 95% C.L. one-parameter limits on anomalous couplings $\Delta\kappa_\gamma$, $\Delta\lambda$ and Δg_1^Z in selected $WW/WZ \to l\nu jj$ data (for combined **electron+muon** channels) obtained from assuming the "LEP Parametrization" and "Equal Couplings" scenarios for $\Lambda_{NP} = 2$ TeV.

68% C.L.	κ_γ	$\lambda_\gamma = \lambda_Z = \lambda$	g_1^Z
LEP Parameterization	$\kappa_\gamma = 1.07^{+0.33}_{-0.22}$	$\lambda = 0.00^{+0.06}_{-0.06}$	$g_1^Z = 1.04^{+0.13}_{-0.05}$
Equal Couplings	$\kappa_\gamma = \kappa_Z = 1.04^{+0.15}_{-0.07}$	$\lambda = 0.00^{+0.06}_{-0.06}$	-
95% C.L.	$\Delta\kappa_\gamma$	$\Delta\lambda_\gamma = \Delta\lambda_Z = \Delta\lambda$	Δg_1^Z
LEP Parameterization	-0.44 < $\Delta\kappa_\gamma$ < 0.55	-0.10 < $\Delta\lambda$ < 0.11	-0.12 < Δg_1^Z < 0.20
Equal Couplings	-0.16 < $\Delta\kappa$ < 0.23	-0.11 < $\Delta\lambda$ < 0.11	-

TABLE IV: Comparison of 95% C.L. one-parameter TGC limits from DØ between the different channels: $WW \to l\nu l\nu$, $W\gamma \to l\nu\gamma$, $WZ \to lll\nu$ and $WW + WZ \to l\nu jj$ ($l = \mu, e$) at $\Lambda_{NP} = 2$ TeV.

LEP Parameterization	$\Delta\kappa_\gamma$	$\Delta\lambda_\gamma = \Delta\lambda_Z = \Delta\lambda$	Δg_1^Z
$WZ \to l\nu ll$ (1/fb)	-	$-0.17 < \Delta\lambda < 0.21$	$-0.14 < \Delta g_1^Z < 0.34$
$W\gamma \to l\nu\gamma$ (0.75/fb)	$-0.51 < \Delta\kappa_\gamma < 0.51$	$-0.12 < \Delta\lambda < 0.13$	-
$WW \to l\nu l\nu$ (1.0/fb)	$-0.54 < \Delta\kappa_\gamma < 0.83$	$-0.14 < \Delta\lambda < 0.18$	$-0.14 < \Delta g_1^Z < 0.30$
$WW + WZ \to l\nu jj$ (1/fb)	$-0.44 < \Delta\kappa_\gamma < 0.55$	$-0.10 < \Delta\lambda < 0.11$	$-0.12 < \Delta g_1^Z < 0.20$
Equal Couplings	$\Delta\kappa_\gamma$	$\Delta\lambda_\gamma = \Delta\lambda_Z = \Delta\lambda$	Δg_1^Z
$WZ \to l\nu ll$ (1/fb)	-	$-0.17 < \Delta\lambda < 0.21$	-
$W\gamma \to l\nu\gamma$ (0.75/fb)	-	$-0.12 < \Delta\lambda < 0.13$	-
$WW \to l\nu l\nu$ (1/fb)	$-0.12 < \Delta\kappa < 0.35$	$-0.14 < \Delta\lambda < 0.18$	-
$WW + WZ \to l\nu jj$ (1/fb)	$-0.16 < \Delta\kappa < 0.23$	$-0.11 < \Delta\lambda < 0.11$	-

TABLE V: Measured values of κ_γ, λ and g_1^Z couplings and their errors at 68% C.L. obtained from the one-parameter fits combining data from different topologies and energies at LEP experiments.

68% C.L.	ALEPH	OPAL	L3	DELPHI
κ_γ	0.971±0.063	$0.88^{+0.09}_{-0.08}$	1.013±0.071	$1.25^{+0.22}_{-0.21}$
λ	-0.012±0.029	$-0.060^{+0.034}_{-0.033}$	-0.021±0.039	$0.05^{+0.09}_{-0.09}$
g_1^Z	1.001±0.030	$0.987^{+0.034}_{-0.033}$	0.966±0.036	$0.98^{+0.07}_{-0.07}$

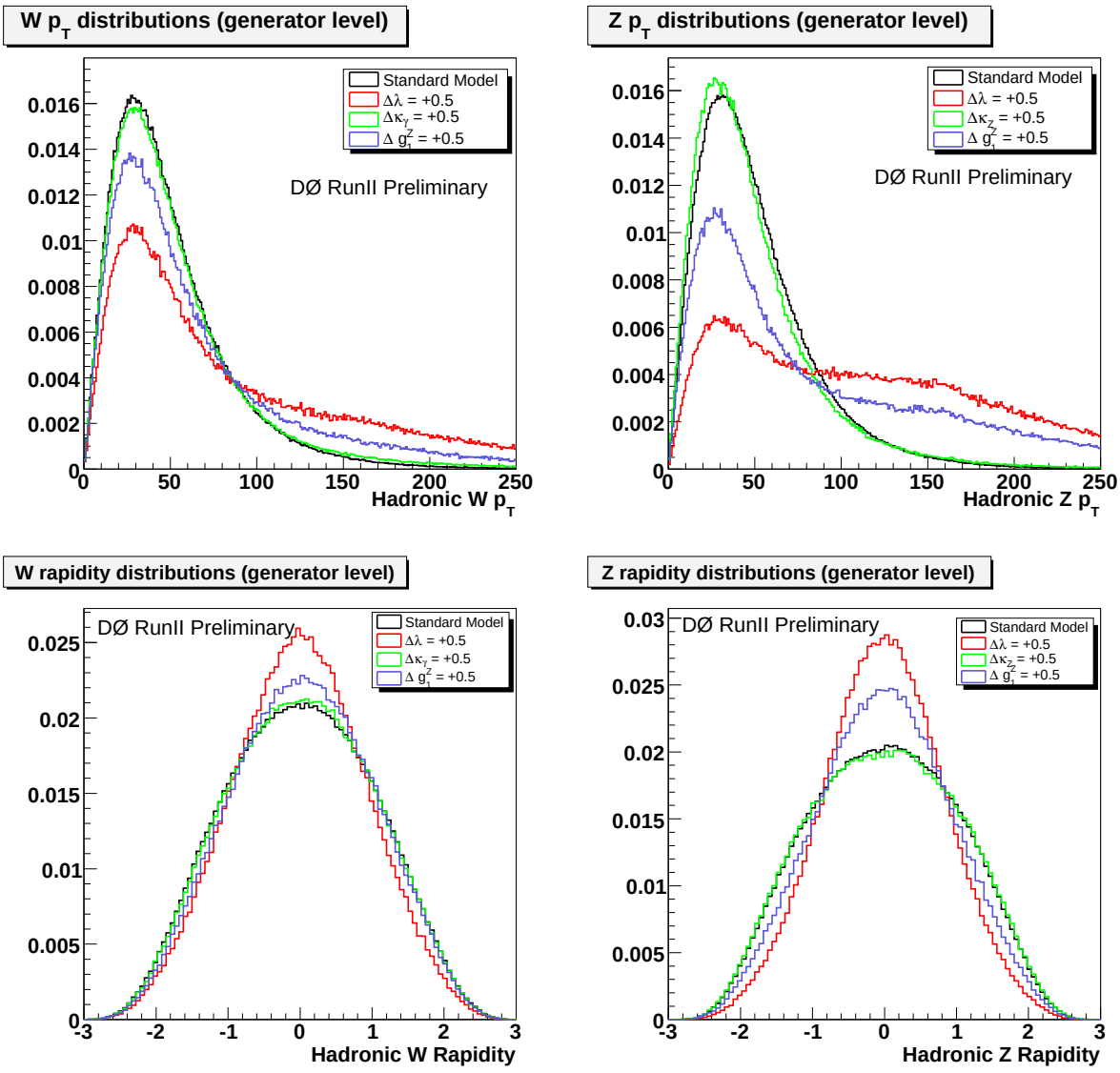

FIG. 2: Distributions of dijet ($W/Z \to q\bar{q}$) p_T and W/Z boson rapidity at the parton level in the presence of the LEP parameterized anomalous couplings $\Delta\kappa_\gamma = +0.5$ (green), $\Delta\lambda = +0.5$ (red) and $\Delta g_1^Z = +0.5$ (blue) compared to the SM (black) distribution for WW production (left) and WZ production (right) with unity normalization. The new physics scale Λ_{NP} is set to 2 TeV.

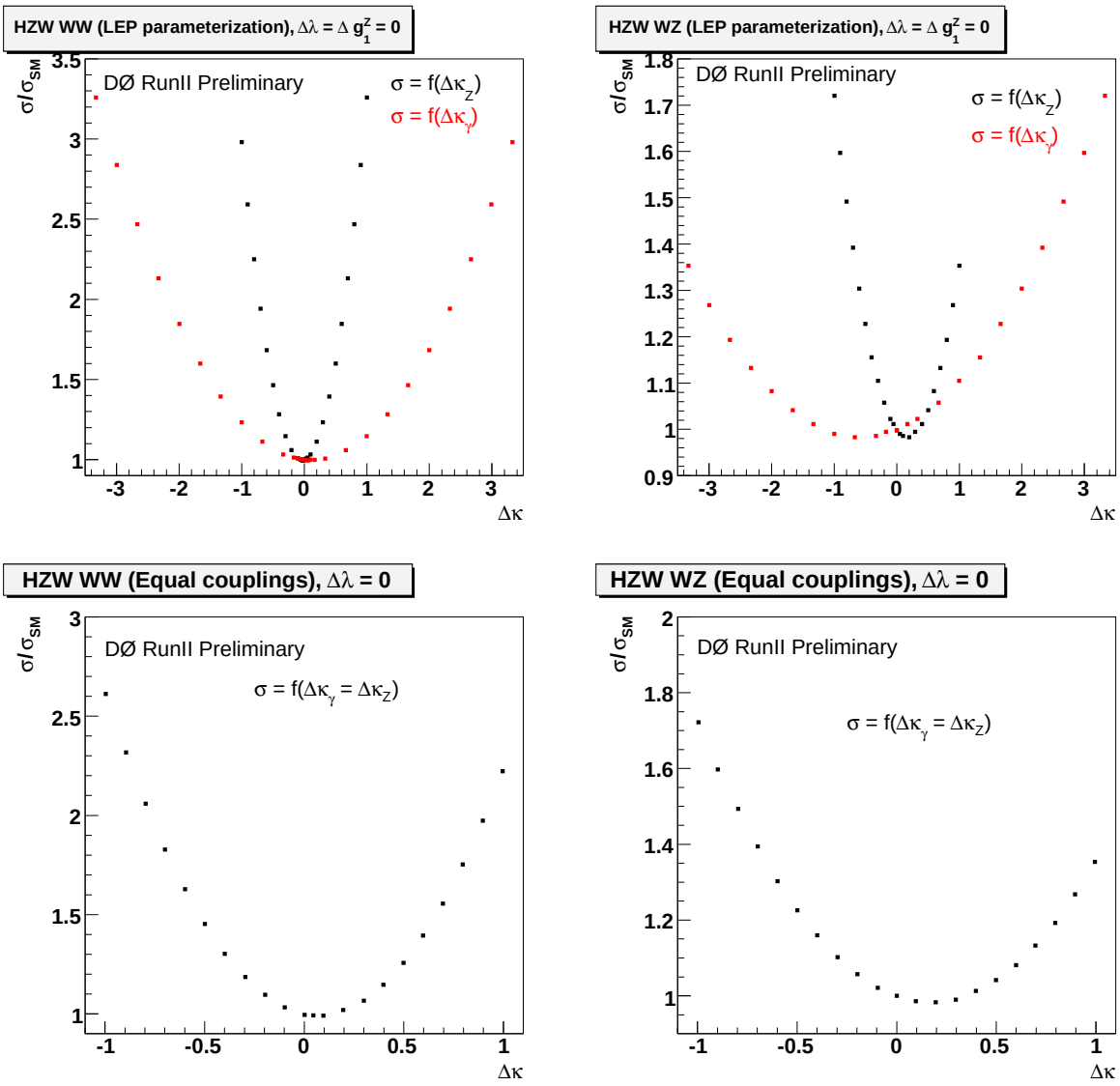

FIG. 3: WW (left) and WZ (right) semileptonic production cross sections normalized to the SM prediction as a function of anomalous couplings $\Delta\kappa$ assuming the "LEP parametrization" scenario (top) and the "Equal couplings" scenario (bottom). The new physics scale Λ_{NP} is set to 2 TeV.

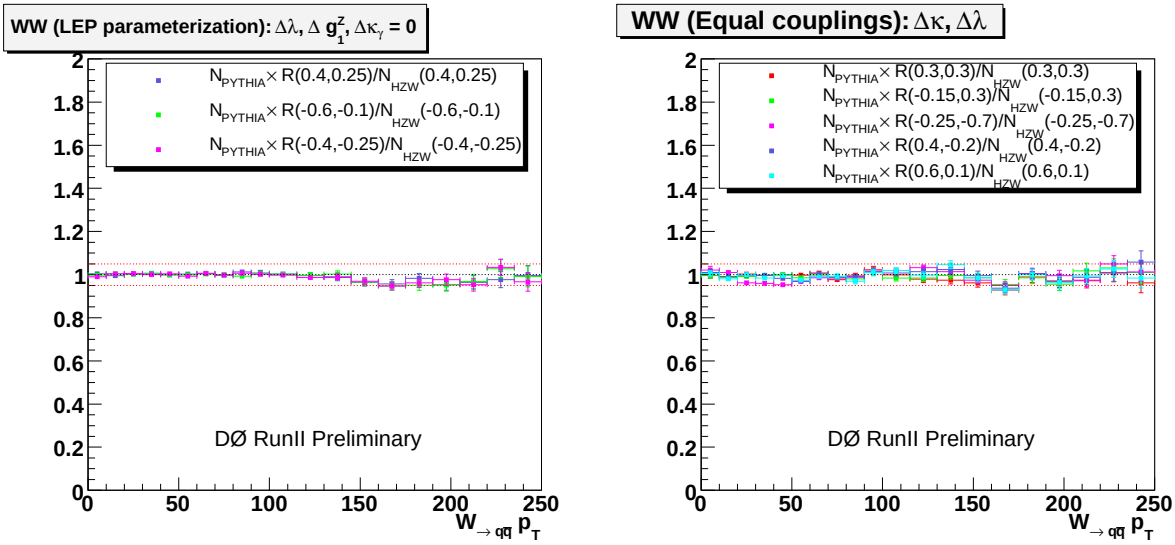

FIG. 4: The shape comparison of the SM PYTHIA WW distributions reweighted by R and distributions predicted by the HZW generator in the presence of different anomalous couplings assuming the "LEP parameterization" (left) and "Equal couplings" (right) scenario. Λ_{NP} is set to 2 TeV. The red lines mark the $\pm 5\%$ condition.

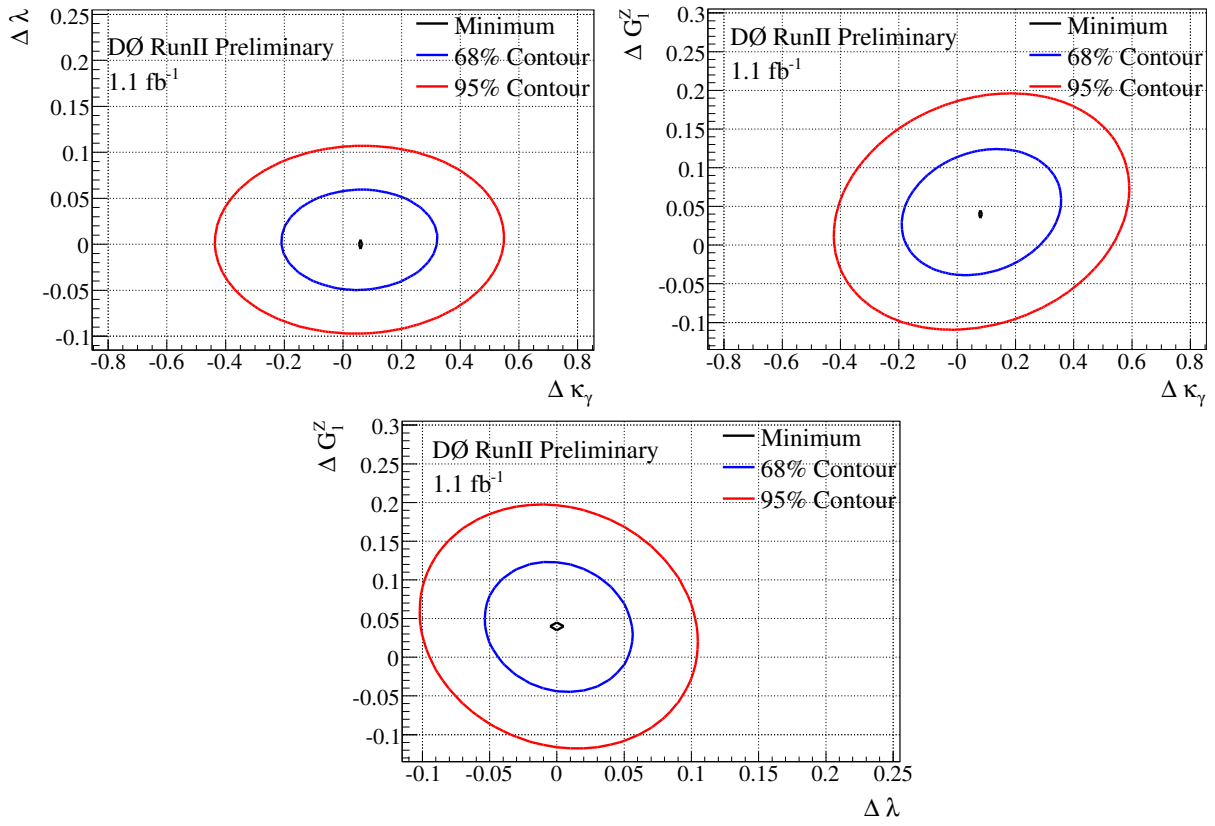

FIG. 5: The 68% C.L. (blue) and 95% C.L. (red) two-parameter limits on the $\gamma WW/ZWW$ coupling parameters $\Delta\kappa_\gamma$, $\Delta\lambda$ and Δg_1^Z, assuming the "LEP parametrization" scenario and $\Lambda_{NP} = 2$ TeV. Black dots indicate the most probable values of anomalous couplings from the two-parameter combined (**electron+muon**) fit.

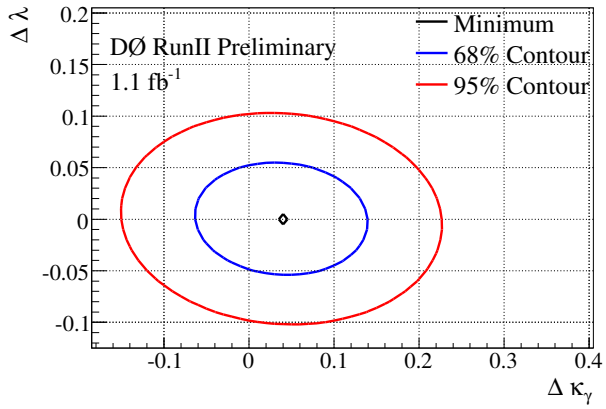

FIG. 6: The 68% C.L. (blue) and 95% C.L. (red) two-parameter limits on the $\gamma WW/ZWW$ coupling parameters $\Delta\kappa$ and $\Delta\lambda$, assuming the "Equal couplings" scenario and $\Lambda_{NP} = 2$ TeV. Black dots indicate the most probable value of anomalous couplings from the two-parameter combined (**electron+muon**) fit.

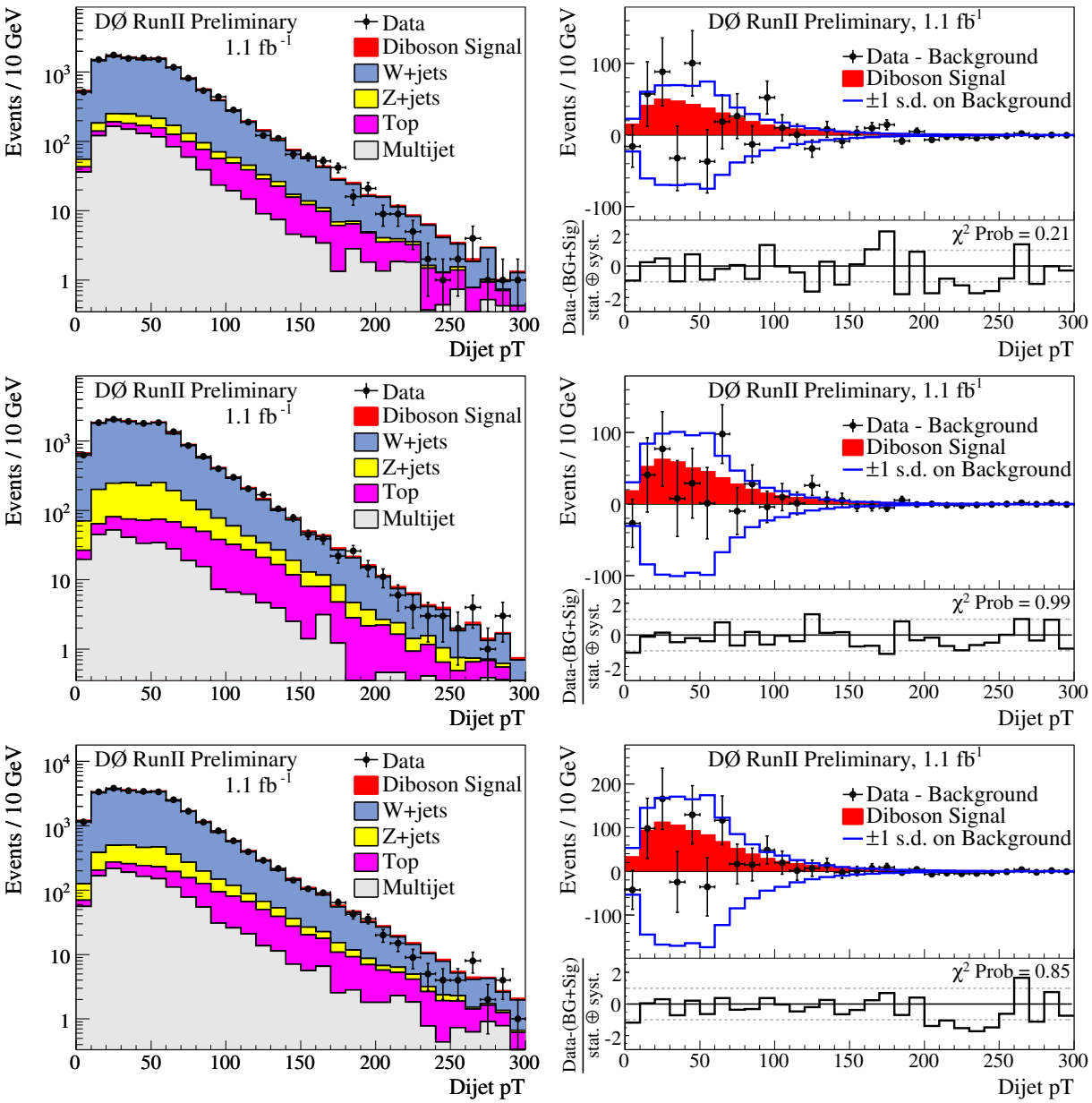

FIG. 7: *Left*: The dijet p_T distributions from the electron (top), muon (middle) and combined channels (bottom) for data and MC predictions following the fit of MC to data. *Right*: A comparison of the extracted signal (filled histogram) to background-subtracted data (points), along with the ±1 standard deviation (s.d.) systematic uncertainty on the background. The residual distance between the data points and the extracted signal, divided by the total uncertainty on the MC, is given at the bottom.

Acknowledgments

We thank the staffs at Fermilab and collaborating institutions, and acknowledge support from the DOE and NSF (USA); CEA and CNRS/IN2P3 (France); FASI, Rosatom and RFBR (Russia); CNPq, FAPERJ, FAPESP and FUNDUNESP (Brazil); DAE and DST (India); Colciencias (Colombia); CONACyT (Mexico); KRF and KOSEF (Korea); CONICET and UBACyT (Argentina); FOM (The Netherlands); STFC and the Royal Society (United Kingdom); MSMT and GACR (Czech Republic); CRC Program, CFI, NSERC and WestGrid Project (Canada); BMBF and DFG (Germany); SFI (Ireland); The Swedish Research Council (Sweden); CAS and CNSF (China); and the Alexander von Humboldt Foundation (Germany).

[1] K. Hagiwara, J. Woodside, and D. Zeppenfeld, Phys. Rev. D **41**, 2113 (1990).
[2] DØ Collaboration: V. M. Abazov *et al.*, Phys. Rev. Lett. **94**, 151801 (2005); Phys. Rev. D **76**, 111104(R) (2007); Phys. Rev. Lett. **101**, 171803 (2008).
[3] CDF Collaboration: D. Acosta *et al.*, Phys. Rev. Lett. **94**, 211801 (2005); A. Abulencia *et al.*, Phys. Rev. Lett. **98**, 161801 (2007); T. Aaltonen *et al.*, Phys. Rev. Lett. **100**, 201801 (2008).
[4] DØ Collaboration: V. M. Abazov *et al.*, "First Evidence for Diboson Production in Lepton Plus Jets Decays," arXiv.org:0810.3873 (2008), accepted by Phys. Rev. Lett.
[5] LEP Collaboration: P. Bambade *et al.*, arXiv:hep-ex/0307056v1 (2003).
[6] B. W. Lee, C. Quigg and H. B. Thacker, Phys. Rev. D **16** (1977); M. S. Chanowitz and M. K. Gaillard, Nucl. Phys. B **261** (1985); M. Chanowitz, M. Golden and H. Georgi, Phys. Rev. D **36** (1987).
[7] K. Hagiwara *et al.*, Nucl. Phys. B **282** (1987).
[8] Z. Ajaltouni *et al.*, "Triple Gauge Boson Couplings," To appear in "Physics at LEP2", G. Altarelli and F. Zwirner eds., CERN Report 1996., hep-ph/9601233v1 (1996).
[9] T. Appelquist and C. Bernard, Phys. Rev. D **22** (1980); C .N. Leung, S. T. Love and S. Rao, Z. Phys. C **31** (1986).
[10] J. Gasser and H. Leutwyler, Ann. Phys. (N.Y.) **158** (1984); Nucl. Phys. B **250** (1985); T. Appelquist and C. Bernard, Phys. Rev. D **22** (1980); A. Longhitano, Phys. Rev. D **22** (1980); Nucl. Phys. B **188** (1981); T. Appelquist and G. H. Wu, Phys. Rev. D **48** (1993).
[11] T. Sjöstrand, *et al.*, Computer Phys. Commun. **135** (2001) 238 (LU TP 00 [arXiv:hep-ph/0010017]).
[12] K. Hagiwara *et al.*, Phys. Rev. D **41** (1990).
[13] W. Fisher, J. Haley and J. Sekaric, DØ Note 5544 (2008).
[14] L. Breiman, Machine Learning **45**, 5 (2001).
[15] I. Narsky, arXiv:physics/0507143 [physics.data-an] (2005).
[16] J. Pumplin, *et al.*, JHEP **0207**, 012 (2002).
[17] F. James, "MINUIT Function Minimization and Error Analysis, Reference Manual," http://wwwasdoc.web.cern.ch/wwwasdoc/minuit/minmain.html
[18] W. Fisher, "Systematics and Limit Calculations," FERMILAB-TM-2386-E.
[19] DØ Collaboration: V. M. Abazov *et al.*, DØ Note 5909-CONF, arXiv.org:0904.0673 (2009), submitted to Phys. Rev. Lett.
[20] DØ Collaboration: V. M. Abazov *et al.*, Phys. Rev. D **76**, 111104(R) (2007).
[21] DØ Collaboration: V. M. Abazov *et al.*, Phys. Rev. Lett. **100**, 241805 (2008).
[22] ALEPH Collaboration: S. Schael *et al.*, Phys. Lett. B **614**, 7 (2005).
[23] OPAL Collaboration: G. Abbiendi *et al.*, Eur. Phys. J. C **33**, 463 (2004).
[24] L3 Collaboration: P. Achard *et al.*, Phys. Lett. B **586**, 151 (2004).
[25] DELPHI Collaboration: P. Abreu *et al.*, CERN-EP/2001-006 (2001).